Interaction Between the Sodium Channel Inactivation Linker and Domain III S4-S5

Marianne R. Smith and Alan L. Goldin
Departments of Microbiology and Molecular Genetics and Physiology and Biophysics, University of California, Irvine, California 92697-4025 USA

ABSTRACT The III-IV linker (L_{III-IV}) of the rat brain sodium channel is critical for fast inactivation, possibly forming a fast inactivation particle. Inactivation can be disrupted by mutation of a conserved alanine at position 1329 in the S4-S5 loop of domain III. Combination of a charged mutation at 1329 with a compensatory (opposite) charge mutation at position 1489 in L_{III-IV} partially restores inactivation of the channel. The compensatory charge mutant channel has a single-channel mean open time that is similar to that of the wild-type channel and is ~50 times shorter than that of the L_{III-IV} mutant channel. The results of thermodynamic cycle analysis indicate that the mutations in domain III S4-S5 and L_{III-IV} have a coupling energy of 2.8 kcal/mol, indicating that the two mutations act interdependently. These data suggest that L_{III-IV} interacts directly with A1329, which may form part of the docking site if L_{III-IV} is a fast inactivation particle.

INTRODUCTION

Voltage-gated sodium channels initiate the rising phase of action potentials that are responsible for signaling throughout the nervous system (Catterall, 1992). Sodium channels open in response to membrane depolarization and then inactivate within 1–2 ms to prevent further flow of sodium ions into the cell. Inactivated channels cannot reopen until the membrane is repolarized and the channels enter the closed state. Abnormalities in fast inactivation can cause defects in electrical excitation, as demonstrated by the mutations in the human skeletal muscle sodium channel gene that cause hyperkalemic periodic paralysis and paramyotonia congenita (McClatchey et al., 1992; Ptacek et al., 1994), and mutations in the cardiac sodium channel gene that cause long QT syndrome (Wang et al., 1995, 1996).

Armstrong and Bezanilla originally proposed a ball-and-chain model to describe sodium channel fast inactivation (Armstrong and Bezanilla, 1977). This type of mechanism has been shown to be true for the *Shaker* potassium channel (Hoshi et al., 1990; Zagotta et al., 1990), in which the cytoplasmic amino terminus functions as an inactivation particle and occludes the pore of the channel. The sodium channel is structurally homologous to the *Shaker* potassium channel. In the sodium channel, the cytoplasmic linker between domains III and IV (L_{III-IV}) is critical for fast inactivation and may form an inactivation particle similar to the *Shaker* amino terminus (Stühmer et al., 1989; Vassilev et al., 1989; Patton et al., 1992; West et al., 1992; Kellenberger et al., 1997a,b). In fact, the sodium channel L_{III-IV} region can function as an inactivation particle when substituted for the amino terminus of the Kv1.1 potassium channel (Patton et al., 1993). Unlike the *Shaker* inactivation particle (Murrell-Lagnado and Aldrich, 1993a,b), the function of the putative sodium channel inactivation particle is not greatly influenced by neutralization of charged amino acids (Moorman et al., 1990; Patton et al., 1992). Rather, three hydrophobic amino acids (IFM) are critical, because replacement of these with polar residues results in channels that do not inactivate (West et al., 1992; Kellenberger et al., 1997b). The essential residue is F1489, which appears to be accessible from the cytoplasmic side at negative membrane potentials, but is inaccessible when the channel is inactivated (Kellenberger et al., 1996). The definitive experiment required to validate the ball-and-chain model for the sodium channel, in which a synthetic peptide inactivates the channel, has been inconclusive. A peptide consisting of KIFMK can function to occlude the channel when applied to the cytoplasmic side of the channel (Eaholtz et al., 1994), but the properties of that process are not identical to those observed during normal channel inactivation (Tang et al., 1996).

If the sodium channel inactivates by a ball-and-chain mechanism, then a region of the channel must function as a docking site for the inactivation particle. In the *Shaker* channel, mutations that neutralize polar and charged residues in the S4-S5 linker disrupt inactivation, suggesting that this region may act as a docking site for the *Shaker* particle (Isacoff et al., 1991). In the sodium channel, hydrophobic residues in the S4-S5 linker of domain III (Yang et al., 1994) or IV (Tang et al., 1996) and the S6 transmembrane segment of domain IV (McPhee et al., 1994, 1995) have been shown to be important for inactivation. However, a direct interaction between L_{III-IV} and any proposed docking site has not been demonstrated. In this study, we identify a residue in domain III S4-S5 of the rat brain type IIA sodium channel that interacts with L_{III-IV}, consistent with a model in which it forms part of a docking site.

Received for publication 11 March 1997 and in final form 23 June 1997.
Address reprint requests to Dr. Alan L. Goldin, Department of Microbiology and Molecular Genetics, University of California, Irvine, CA 92697-4025. Tel.: 714-824-5334; Fax: 714-824-8598; E-mail: agoldin@uci.edu.

0006-3495/97/10/1885/11 $2.00

MATERIALS AND METHODS

Site-directed mutagenesis

The plasmid pVA2580 contains the rat brain IIA (RIIA) sodium channel coding region downstream from a T7 RNA polymerase promoter (Auld et al., 1990). The domain II and III S4-S5 regions of RIIA, as defined by the unique restriction sites *XmaI* and *BglII* for domain II, and *BglII* and *BstEII* for domain III, were subcloned into M13 mp18A, a version of M13 mp18 with a polylinker region that was modified to contain unique restriction sites in the RIIA coding region. M13 single-strand mutagenesis was used to create the mutations, as previously described (Smith and Goldin, 1996). Uracil-containing, single-stranded DNA was isolated from phage grown in the *dut⁻ ung⁻ Escherichia coli* strain RZ1032 in YT media supplemented with 250 μg/ml uridine. Each mutagenic oligonucleotide primer (shown below) was kinased with T4 polynucleotide kinase and annealed to the template at a 10:1 molar ratio. The primer was extended with T7 DNA polymerase (2.5 units) in the presence of T4 DNA ligase (6 Weiss units) in a 100-μl reaction containing 10 mM $MgCl_2$, 0.5 mM deoxynucleotide triphosphates, 1 mM ATP, 2 mM dithiothreitol, and 20 mM Tris-HCl, pH 7.5. The reaction mixture was incubated first on ice for 5 min, then at room temperature for 5 min, and finally at 37°C for 2 h. XL-1 bacteria were transformed with the heteroduplex DNA by electroporation and plated with XL-1 lawn cells. Individual plaques were picked and plaque purified before phage was grown, to isolate single-stranded DNA, which was used to screen for the mutation by dideoxynucleotide sequencing. Double-stranded replicative form DNA was isolated and used to ligate the sodium channel region containing the mutation back into the plasmid containing the full-length coding region.

Mutations were constructed using the following oligonucleotide primers:

LNM867-69Q3:
CGATGATCTTAATGAGCTGCTGCTGTGTGGGCCAGGACTTTGC
LIK870-72Q3:
CGAGTTGCCGATGATCTGCTGCTGCATGTTCAGTGTGGG
IIG873-75Q3: CCCACCGAGTTCTGCTGCTGCTTAATGAGC
NSV876-78Q3:
GTTGCCCAGTGCACCCTGCTGCTGGCCGATGATCTTAATGAGC
GAL879-81Q3:
GGTCAGGTTGCCCTGTTGCTGCACCGAGTTGCC
GN882-83Q2: GCACCAGGGTCAGCTGCTGCAGTGCACCC
VVV1325-27Q3:
CGCCTAAGAGAGCGTTGTGCTGCTGCCTGATTCCTTC
N1328Q: GCCTAAGAGAGCCTGTACAACAACCCTC
ALL1329-31Q3:
GGAGGGGATGGCGCCGTGCTGCTGGTTTACAACAACCCT
IPS1334-36Q3:
AAGTACGTTCATTATCTGCTGCTGGGCGCCTAAGAGAGC
V1327K: GCCTAAGAGAGCGTTTTTAACAACCCTCATTCC
A1329Q: GCCTAAGAGCTGGTTTACAACAACC
A1329K: GCCTAAGAGTTTGTTTACAACAACC
A1329D: GCCTAAGAGGTCGTTTACAACAACC
A1329R: GCCTAAGAGACGGTTTACAACAACC
A1329E: GCCTAAGAGCTCGTTTACAACAACC
L1330Q: GGCGCCTAACTGAGCGTTTAC
L1331Q: GATGGCGCCCTGGAGAGCG
L1331K: GGGGATGGCGCCTTTGAGAGCGTTTAC
F1489D: GTTCTTCTGTCATGTCGATGTCTTGACC
F1489K: CTGTTCTTCTGTCATCTTGATGTCTTGACC
F1489E: GTTCTTCTGTCATCTCGATGTCTTGACC
F1489R: CTGTTCTTCTGTCATCCTGATGTCTTGAAC

Oocyte expression and electrophysiological analysis

RNA transcripts were synthesized from *NotI* linearized DNA templates using the T7 mMESSAGE mMACHINE kit (Ambion, Austin, TX). Stage V oocytes were removed from adult female *Xenopus laevis* frogs, prepared as previously described (Goldin, 1991) and incubated in ND-96 media (96 mM NaCl, 2 mM KCl, 1.8 mM $CaCl_2$, 1 mM $MgCl_2$, and 5 mM HEPES, pH 7.5), supplemented with 0.1 mg/ml gentamicin, 0.55 mg/ml pyruvate, and 0.5 mM theophylline. Sodium channel α-subunit RNA and sodium channel β_1-subunit RNA were coinjected into oocytes at an approximate molar ratio of 1α:$10\beta_1$ to attain current levels of 1–4 μA, 1–3 days after injection. After incubation at 20°C in ND-96 for 1–3 days, sodium currents were recorded at room temperature with a two-electrode voltage clamp as previously described (Patton and Goldin, 1991). The bath recording solution consisted of ND-96. Currents were measured and analyzed with pCLAMP software (version 6.0.3; Axon Instruments, Burlingame, CA). All analyses, except for recovery from inactivation, were performed after subtraction of currents recorded in the presence of 400 nM tetrodotoxin.

Currents were recorded at a depolarization of −10 mV to measure inactivation time constants and maintained currents. Time constants were determined by using the Chebyshev method to fit the current traces with a single exponential equation, $A1 * \exp[-(t - K)/\tau 1] + C$, or a double-exponential equation, $A1 * \exp[-(t - K)/\tau 1] + A2 * \exp[-(t - K)/\tau 2] + C$, where A1 and A2 represent the proportion of channels inactivating with time constants $\tau 1$ and $\tau 2$, K is the time shift, and C is the steady-state asymptote. The time shift was manually selected by fitting the traces at the time when the currents were just starting to decrease exponentially. Maintained current was calculated by dividing the current amplitude either 14 ms (Table 1) or 200 ms (Table 2) after the initiation of the depolarization by the maximum current amplitude. K_{on} and K_{off} were calculated using the equations $K_{on} = (1 - I_{ss})/\tau_f$ and $K_{off} = I_{ss}/\tau_f$, where I_{ss} is the ratio of steady-state to peak current, and τ_f is the time constant for the fast component of inactivation. The free energy of inactivation (ΔG) was calculated by using the equation $\Delta G = -RT \ln(K_{eq})$, where R is the universal gas constant, T is temperature, and $K_{eq} = K_{on}/K_{off}$.

Oocytes were clamped at a holding potential of −100 mV and currents were elicited by 18-ms depolarizations ranging from −90 mV to +55 mV in 5-mV increments to determine the voltage dependence of conductance. Conductance values were calculated using the formula $G = I/(V - V_r)$, where G is conductance, I is current amplitude, V is the depolarized membrane potential, and V_r is the reversal potential for sodium. Reversal potentials were individually estimated for each data set by fitting the I-V data as previously described (Kontis and Goldin, 1993). Conductance values were fit with a two-state Boltzmann equation, $G = 1/(1 + \exp[-0.03937 * z * (V - V_{1/2})])$, where z is the apparent gating charge, V is the command potential, and $V_{1/2}$ is the voltage required for half-maximum activation.

The voltage dependence of steady-state inactivation was determined by using 1-s conditioning prepulses from −100 mV to 15 mV in 5-mV increments, followed by a test pulse to −5 mV for 24.8 ms. Long prepulses (1 s) were necessary to obtain significant inactivation of the mutant channels that inactivated very slowly. Peak current amplitudes measured during the test depolarization were normalized to the maximum current amplitude and are plotted as a function of the conditioning prepulse potential. The data were fit with a two-state Boltzmann equation, $I = 1/(1 + \exp[0.03937 * z * (V - V_{1/2})])$, where I is current, z is the apparent gating charge, V is the prepulse depolarization potential, and $V_{1/2}$ is the voltage depolarization required for half-maximum inactivation.

To measure recovery from inactivation, oocytes were held at −100 mV. One-second prepulses to −10 mV were followed by variable recovery periods from 200 ms to 2 ms or from 1500 ms to 10 ms at −100 mV, followed by 15-ms test pulses to −10 mV. Long prepulses (1 s) were necessary to obtain significant inactivation of the mutant channels that inactivated very slowly. Peak current amplitudes during the test pulse were normalized to the current amplitude of a 70-ms pulse to −10 mV elicited before the recovery protocol, and plotted as a function of the duration of the recovery interval. The data for A1329D and A1329D/F1489K were fit to a double exponential equation, $1 - [(a * \exp(-t/\tau 1) + b * \exp(-t/\tau 2)]$, and the data for all of the other channels were fit to a triple exponential equation, $1 - [(a * \exp(-t/\tau 1) + b * \exp(-t/\tau 2) + c * \exp(-t/\tau 3)]$, where a, b, and c represent the proportion of recovery with time constants $\tau 1$, $\tau 2$, and $\tau 3$, respectively, and t is the recovery interval. The slowest time

TABLE 1 Inactivation kinetics for mutations identifying regions that disrupt fast inactivation

Channel	Inactivation time constants: Fast component (ms)	Percentage of fast component	Slow component (ms)	Percentage of slow component	Maintained current (14 ms)	*n*
Wild type	1.1 ± 0.2	94 ± 2%	14.0 ± 0.4	6 ± 2%	4 ± 1%	5
LNM867-69Q3	1.4 ± 0.4	ND	ND	ND	3 ± 1%	6
LIK870-72Q3	1.0 ± 0.3	96 ± 2%	15.6 ± 0.6	4 ± 2%	2.1 ± 0.4%	5
IIG873-75Q3	1.5 ± 0.4	95 ± 2%	14.0 ± 0.8	5 ± 2%	4 ± 2%	5
NSV876-78Q3	1.1 ± 0.1	88 ± 2%	14.8 ± 0.5	12 ± 2%	4 ± 1%	6
GAL879-81Q3	1.6 ± 0.2	82 ± 1%	15.2 ± 0.3	18 ± 1%	10 ± 1%	6
GN882-83Q2	1.2 ± 0.1	88 ± 2%	12.9 ± 0.5	12 ± 1%	5 ± 1%	5
VVV1325-27Q3	1.2 ± 0.1	ND	ND	ND	5 ± 3%	5
N1328Q	0.8 ± 0.1	95 ± 1%	11.8 ± 1.4	5 ± 1%	3 ± 1%	5
ALL1329-31Q3	**1.4 ± 0.1**	**84 ± 2%**	**73 ± 8**	**16 ± 2%**	**16 ± 2%**	**5**
GA1332-33Q2	1.2 ± 0.1	96 ± 2%	55 ± 5	4 ± 2%	6 ± 3%	5
IPS1334-36Q3	0.9 ± 0.1	96 ± 2%	15.9 ± 0.9	4 ± 2%	2 ± 1%	5
A1329Q	**1.4 ± 0.1**	**88 ± 1%**	**43 ± 2**	**12 ± 1%**	**18 ± 3%**	**5**
L1330Q	0.5 ± 0.2	ND	ND	ND	1.3 ± 0.3%	5
L1331Q	1.1 ± 0.02	ND	ND	ND	1.6 ± 0.1%	5

ND, Not determined because current traces for these channels were best fit with a single exponential equation.
The mutant channels indicated in bold type in boxes are the focus of the experiments presented in this study.

constant was greater than 2.5 s, and could not be accurately quantified because the longest recovery interval that was used was 1.5 s. This time constant most likely reflected recovery from slow inactivation, and it is not shown in Table 3.

Single-channel recordings were acquired from inside-out patches in an internal bath solution consisting of 88 mM KCl, 9.6 mM NaCl, 1 mM $MgCl_2$, 1 mM $CaCl_2$, 11 mM EGTA, 5 mM HEPES, pH 7.5. Normal frog Ringer's solution (115 mM NaCl, 2.5 mM KCl, 1.8 mM $CaCl_2$, 10 mM HEPES, pH 7.5) was used as the external pipette solution. Currents were recorded with a sampling frequency of 20 kHz and a filter frequency of 2 kHz. Single-channel data were analyzed with pCLAMP 6.0.2 software. The mean open time was determined by fitting dwell-time histograms with the probability density function $f(t) = (1/\tau)\exp(-t/\tau)$, using the simplex least-squares method, where t is equal to time and τ is the mean open time. The transition rate constant is the reciprocal of the mean open time. Five oocytes were used for each determination.

RESULTS

Mutations in III S4-S5 affect fast inactivation

Site-specific mutagenesis was used to scan cytoplasmic regions of the rat brain type IIA (RIIA) sodium channel to identify residues that might be involved in sodium channel fast inactivation. Amino acids in the S4-S5 linkers of domains II and III were substituted with glutamines (Q) in an attempt to disrupt hydrophobic interactions between the putative IFM inactivation particle in L_{III-IV} and the potential docking site for the fast inactivation particle (Fig. 1 *A*). Mutant channels were coexpressed with the sodium channel β_1-subunit (Isom et al., 1992) in *Xenopus* oocytes, and the

TABLE 2 Inactivation kinetics for compensatory charge mutations

Channel	Inactivation time constants: Fast component (ms)	Percentage of fast component	Slow component (ms)	Percentage of slow component	Maintained current	K_{on} (ms^{-1})	K_{off} (ms^{-1})	Mean open time (ms)	Transition rate constant (ms^{-1})
Wild type	1.1 ± 0.2	94 ± 2%	14 ± 0.4	6 ± 2%	1.0 ± 0.9%	0.91 ± 0.17	0.009 ± 0.008	0.3	3
A1329K	1.6 ± 0.2	88 ± 2%	43 ± 1.0	12 ± 2%	10 ± 2%	0.56 ± 0.07	0.06 ± 0.01	0.2	5
F1489D	2.0 ± 0.3	25 ± 5%	262 ± 22	75 ± 5%	72 ± 4%	0.14 ± 0.03	0.36 ± 0.06	9.6	0.1
A1329K/F1489D	1.4 ± 0.1	76 ± 4%	97 ± 3	24 ± 4%	21 ± 4%	0.58 ± 0.08	0.15 ± 0.02	0.2	5
A1329D	1.7 ± 0.2	90 ± 2%	22 ± 0.6	10 ± 2%	1.4 ± 0.5%	0.60 ± 0.08	0.008 ± 0.002	ND*	ND*
F1489K	4.5 ± 1.0	9 ± 2%	241 ± 10	91 ± 2%	70 ± 2%	0.07 ± 0.02	0.16 ± 0.03	ND*	ND*
A1329D/F1489K	ND#	ND#	190 ± 11	ND#	48 ± 2%	ND#	ND#	ND*	ND*
V1327K/F1489D	10 ± 2	16 ± 3%	58 ± 7	84 ± 3%	13 ± 4%	0.09 ± 0.02	0.013 ± 0.003	ND*	ND*
L1331K/F1489D	4.0 ± 0.7	11 ± 3%	86 ± 10	89 ± 3%	17 ± 1%	0.21 ± 0.04	0.04 ± 0.01	ND*	ND*
A1329R	0.9 ± 0.1	95 ± 2%	22 ± 2	5 ± 2%	1.7 ± 0.9%	1.1 ± 0.1	0.018 ± 0.009	ND*	ND*
F1489E	ND#	ND#	176 ± 13	ND#	48 ± 2%	ND#	ND#	ND*	ND*
A1329R/F1489E	7.1 ± 2.0	8 ± 1%	65 ± 12	92 ± 1%	11 ± 3%	0.13 ± 0.03	0.02 ± 0.01	ND*	ND*
A1329E	1.4 ± 0.2	84 ± 5%	90 ± 8	16 ± 5%	10 ± 4%	0.63 ± 0.10	0.07 ± 0.01	ND*	ND*
F1489R	4.8 ± 0.7	9 ± 1%	190 ± 15	91 ± 1%	55 ± 3%	0.09 ± 0.02	0.12 ± 0.02	ND*	ND*
A1329E/F1489R	3.1 ± 0.8	21 ± 5%	123 ± 7	79 ± 5%	29 ± 2%	0.24 ± 0.06	0.10 ± 0.02	ND*	ND*

*Not determined.
#Not determined because current traces for these channels were best fit with a single exponential equation so that there was no fast component.

TABLE 3 Voltage dependence and recovery from inactivation for compensatory charge mutations

	Conductance			Voltage dependence of inactivation			Recovery from inactivation				
Channel	$V_{1/2}$ (mV)	z (e_o)	n	$V_{1/2}$ (mV)	z (e_o)	n	Fast component (ms)	Percentage of fast component*	Slow component (ms)	Percentage of slow component*	n
Wild type	−19 ± 2	5.6 ± 0.6	7	−49 ± 1	5.3 ± 0.1	5	5 ± 2	57 ± 4%	50 ± 13	34 ± 4%	6
A1329K	−10 ± 3	4.3 ± 0.6	6	−40 ± 1	4.8 ± 0.5	6	9 ± 2	25 ± 5%	152 ± 30	61 ± 7%	6
F1489D	−21 ± 2	7.2 ± 0.8	7	ND#	ND#	ND#	ND#	ND#	ND#	ND#	ND#
A1329K/F1489D	−14 ± 3	4.3 ± 0.8	6	−32 ± 1	4.2 ± 0.7	5	12 ± 4	5 ± 2%	148 ± 10	82 ± 5%	5
A1329Q	−12 ± 2	4.3 ± 0.5	8	−38 ± 1	4.2 ± 0.2	6	12 ± 4	23 ± 3%	198 ± 28	63 ± 4%	5
A1329D	−17 ± 2	4.7 ± 0.6	7	−45 ± 2	5.1 ± 0.2	6	4 ± 1	54 ± 2%	94 ± 27	47 ± 3%	6
F1489K	−23 ± 2	6 ± 1	6	ND#	ND#	ND#	ND#	ND#	ND#	ND#	ND#
A1329D/F1489K	−26 ± 2	6.2 ± 0.8	4	−33 ± 2	5.1 ± 0.9	7	ND#	ND§	130 ± 15	66 ± 2%	5

*Less than 100% of the total current recovered from inactivation for all of the channels except A1329D. The remaining current recovered with a time constant that was greater than 2.5 s, and could not be accurately quantified because the longest recovery interval that was used was 1.5 s.
#Not determined because these channels could not be inactivated by a 1-s prepulse.
§Not determined because recovery for these channels was best fit with a double-exponential equation. The second time constant was greater than 2.5 s and could not be accurately quantified because the longest recovery interval that was used was 1.5 s.

electrophysiological properties of the channels were examined by the two-electrode voltage-clamp technique. Inactivation time constants and the percentage of maintained current for the mutant channels are shown in Table 1. Most of the mutant channels inactivated with kinetics similar to those of the wild-type channel. However, the ALL1329-31Q3 mutant in domain III S4-S5 inactivated significantly slower than the wild-type channel, with a pedestal of current maintained for more than 200 ms (Fig. 1 *B* and Table 1). The mutant channel GAL879-81Q3 in domain II S4-S5 also inactivated more slowly than the wild-type channel, in that a greater percentage of current through that channel inactivated with the slow time constant (Table 1). However, this effect was much smaller than that seen for ALL1329-31Q3, so in this study we have focused on analyzing the importance of the ALL1329-31 region for sodium channel fast inactivation.

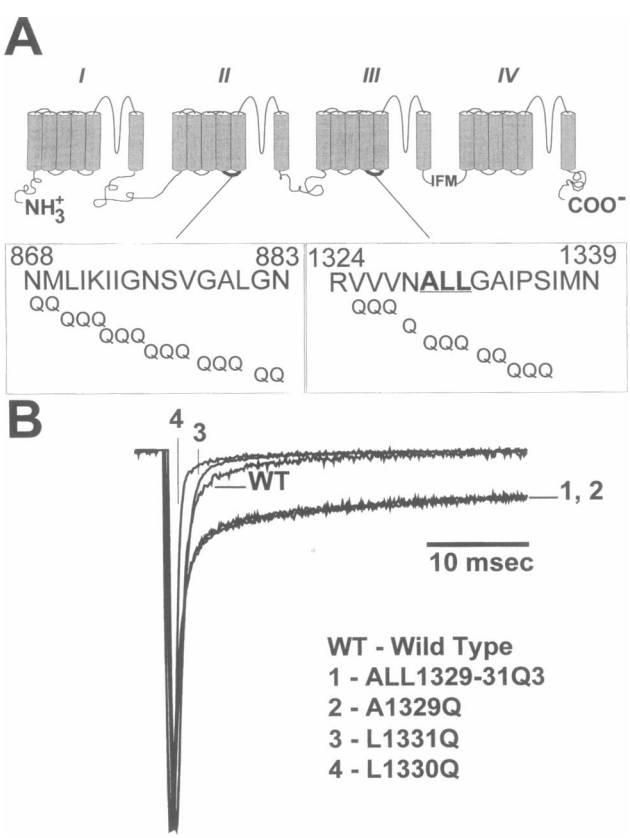

FIGURE 1 Mutations to identify regions that disrupt fast inactivation. (*A*) Diagram of the rat brain IIA sodium channel (RIIA), showing single, double, and triple amino acid mutations to glutamine in the S4-S5 linkers of domains II and III and the location of the IFM inactivation particle in L_{III-IV}. (*B*) Representative current traces at a depolarization of −10 mV are shown for wild type (WT), ALL1329-31Q3 (*trace 1*), A1329Q (*trace 2*), L1331Q (*trace 3*), and L1330Q (*trace 4*).

Three single amino acid substitutions were made at ALL1329 to identify the specific residue that caused slower inactivation. L1330Q inactivated with kinetics slightly faster than those of the wild-type channel, and L1331Q inactivated with kinetics similar to those of the wild-type channel (Fig. 1 *B* and Table 1). The A1329Q mutant showed a slower inactivation time course similar to that of ALL1329-31Q3 (Fig. 1 *B* and Table 1). The alanine at position 1329 is invariant in voltage-gated sodium channels from vertebrates and invertebrates, with the single exception of a sodium channel from jellyfish (Goldin, 1995). The high level of conservation of this residue is consistent with a critical role for some aspect of normal sodium channel function, such as fast inactivation.

Mutations in III S4-S5 can compensate for a mutation in L_{III-IV}

Inactivation of the sodium channel has been modeled as occurring through hydrophobic interactions between the putative IFM inactivation particle and a receptor. Previous studies suggested that phenylalanine (F) at position 1489 in L_{III-IV} forms the nucleus of this particle (West et al., 1992).

Inactivation can be disrupted by substituting a charged residue at this position. If A1329 in domain III S4-S5 normally interacts with F1489 through a hydrophobic interaction, then a mutant channel containing both a charge at 1489 and a compensatory (opposite) charge at 1329 might be able to partially inactivate through electrostatic interactions between the two charges (Fig. 2). This hypothesis was tested by constructing the mutant channels A1329K/F1489D, A1329D/F1489K, A1329R/F1489E, and A1329E/F1489R.

Fig. 3, *A* and *B*, show representative current traces for channels containing single-charge lysine (K) or aspartate (D) substitutions or compensatory combinations of the two charges. Current traces for F1489D and F1489K show that inactivation was almost completely removed when a charge was placed at this position in L_{III-IV}. In contrast, A1329K/F1489D demonstrated a fast component of inactivation that was similar to that of the wild-type channel (Fig. 3 *A* and Table 2). F1489D inactivated more slowly and demonstrated more than twice the maintained current compared to A1329K/F1489D (Table 2). A calculated "on" rate for the putative inactivation particle binding to its receptor was increased for A1329K/F1489D compared to F1489D, whereas the "off" rate was decreased (Table 2, K_{on} and K_{off}). When the charges at the two positions were reversed, A1329D/F1489K inactivated faster than F1489K, as shown by the decrease in the slow component of inactivation and the decrease in maintained current for A1329D/F1489K compared to F1489K alone (Fig. 3 *B* and Table 2). These data demonstrate that combining opposite charge mutations at positions 1329 and 1489 partially restored channel inactivation. This effect occurred with either charge orientation, although the kinetics of inactivation were different, depending on the orientation.

To determine if a specific amino acid combination was necessary for restoration of inactivation in the compensatory charge mutant channels, we also constructed mutants containing arginine (R) and glutamate (E) substitutions. Fig. 3, *C* and *D*, shows representative current traces for the channels containing the compensatory charge mutations A1329R/F1489E and A1329E/F1489R and single charge substitutions. A1329R/F1489E inactivated significantly faster than F1489E, as demonstrated by a decrease in the time constant for the slow component of inactivation and the appearance of a fast component of inactivation (Fig. 3 *C* and Table 2). There was also a dramatic decrease in the percentage of maintained current for A1329R/F1489E to less than one-fourth the maintained current of F1489E alone (Table 2). A similar effect was observed when the arginine/glutamate charge substitutions at the two positions were reversed. A1329E/F1489R inactivated more rapidly than F1489R, as shown by a decrease in the slow component of inactivation and a smaller percentage of maintained current (Fig. 3 *D* and Table 2). These data show that combining opposite charges at position 1489 in L_{III-IV} and position 1329 in III S4-S5 was sufficient to restore inactivation, and that this effect did not depend on the specific amino acid combination.

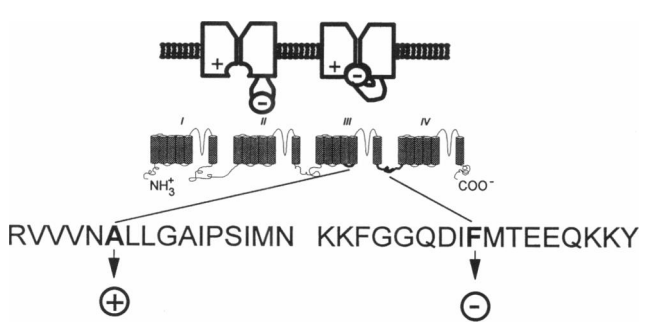

FIGURE 2 Strategy for the compensatory charge mutations. Diagram of the RIIA sodium channel, showing a negative charge mutation at the phenylalanine at position 1489 in L_{III-IV} and a positive charge mutation at the alanine at position 1329 in the S4-S5 linker of domain III.

Mutations in III S4-S5 affect the voltage dependence of activation and inactivation

The S4-S5 linkers are adjacent to the S4 regions that are involved in voltage-dependent channel gating. Therefore it was possible that the mutations could be affecting the voltage dependence of channel gating, and differences in voltage dependence might be reflected by changes in inactivation kinetics. To evaluate this possibility, we examined the voltage dependence of conductance for the various mutants. The $V_{1/2}$ for conductance was shifted in the positive direction for A1329K, A1329Q, and A1329K/F1489D, without any significant change in slope compared to the wild-type channel (Fig. 4, *A* and *B*, and Table 3). In contrast, the conductance curves for F1489K and A1329D/F1489K were shifted in the negative direction compared to that of the wild-type channel. All of these shifts were less than 10 mV. These data show that mutations in the S4-S5 linker of domain III and in L_{III-IV} can have small effects on the voltage dependence of channel activation. However, the shifts in activation could not account for the differences in inactivation kinetics between channels with the compensatory charge mutations and channels with a charge in only the putative inactivation particle.

Because activation and inactivation are coupled in sodium channels, we examined whether the various mutations affected the voltage dependence of steady-state inactivation. The mutant channels F1489D and F1489K were not included because they could not be completely inactivated with a 1-s depolarizing pulse. All of the mutant channels that inactivated more slowly than the wild-type channel had inactivation curves that were shifted in the positive direction relative to that of the wild-type channel (Fig. 4 *C* and Table 3). A1329K and A1329Q inactivated somewhat more slowly than the wild-type channel, and these two mutants had inactivation curves that were shifted by ~10 mV in the depolarizing direction. A1329D/F1489K and A1329K/F1489D inactivated significantly more slowly than the wild-

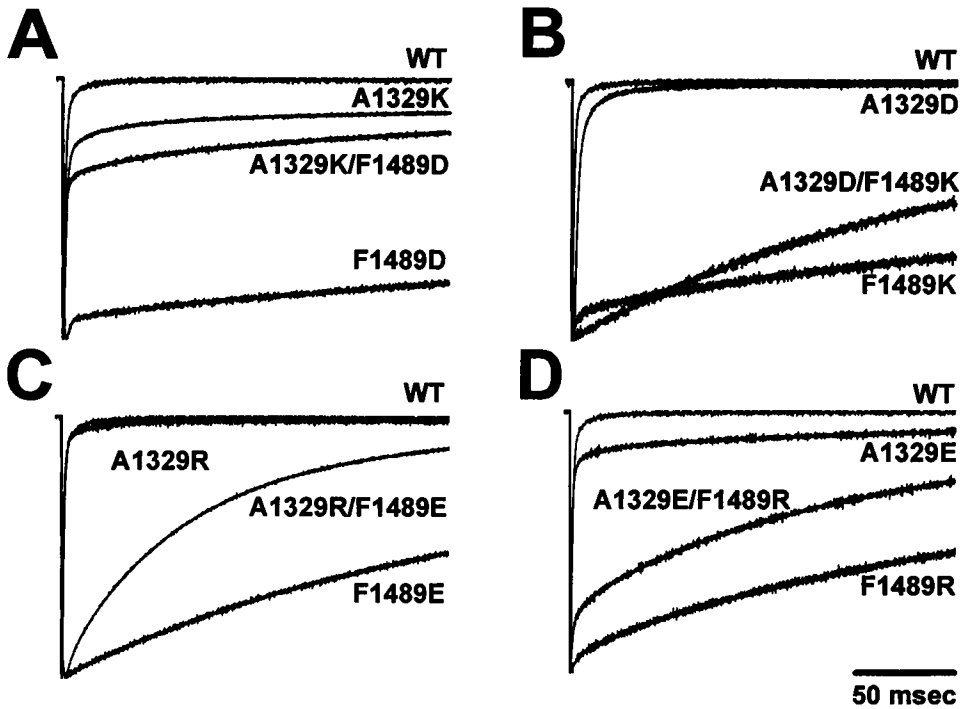

FIGURE 3 Representative current traces at a depolarization of −10 mV for the wild-type (WT) and mutant channels. (*A*) Current traces for A1329K, F1489D, and A1329K/F1489D. (*B*) Current traces for A1329D, F1489K, and A1329D/F1489K. (*C*) Current traces for A1329R, F1489E, and A1329R/F1489E. (*D*) Current traces for A1329E, F1489R, and A1329E/F1489R.

type channel, and these two mutants showed an even larger positive shift of ~16 mV. Therefore, mutations in domain III S4-S5 do affect the voltage dependence of inactivation by shifting the $V_{1/2}$ in the positive direction, and the degree of shift appears to correlate with the extent of slowing of inactivation.

Recovery from inactivation is slower for the compensatory mutants

The stability of the inactivated state can be studied by examining the kinetics of recovery from fast inactivation. Fig. 5 shows recovery from inactivation for the inactivating mutants and wild-type channels. As with the voltage dependence of inactivation, F1489D and F1489K were not included because they could not be completely inactivated with a 1-s depolarization. The data were fit with a double- or triple-exponential equation, as described in Materials and Methods. The third time constant was greater than 2.5 s and most likely reflected recovery from slow inactivation because of the long depolarizing prepulse. The magnitude of this time constant could not be accurately determined because the longest recovery interval was 1.5 s, so the values for this parameter were not included in Table 3. A1329D recovered from inactivation as rapidly as the wild-type channel (Fig. 5 *A* and Table 3), but A1329Q, A1329K, A1329K/F1489D, and A1329D/F1489K all recovered from inactivation significantly more slowly than the wild-type channel (Fig. 5 *B* and Table 3). In particular, A1329D/F1489K demonstrated the slowest recovery from inactivation. These results indicate that the various mutations have decreased the rate of recovery from inactivation, despite the fact that the calculated "off" rate for a putative inactivation particle is faster for these mutants than it is for the wild-type channel (Table 1).

Single-channel analysis of compensatory mutants

To better understand the inactivation kinetics of the mutant channels, single-channel currents were recorded from inside-out patches for the wild-type, A1329K, F1489D, and A1329K/F1489D channels at a membrane depolarization of −10 mV (Fig. 6). The majority of the wild-type channel openings occurred at the beginning of the depolarization, with very few reopenings during the remainder of the depolarization and a short mean open time of 0.3 ms (Table 2). A1329K also opened at the beginning of the depolarization and closed quickly, with a mean open time of 0.2 ms, but this channel frequently reopened two or three times during the remainder of the depolarization. There is no significant difference between an open time of 0.2 or 0.3 ms with the conditions we used for recording, because the briefest opening that can be quantified with a 2-kHz filter is 0.16 ms. F1489D had very long open times, with a mean open time of 9.6 ms, and continuously reopened throughout the depolarization. The ensemble average for F1489D shows that the open probability is nearly at maximum throughout the depolarization. In contrast, A1329K/F1489D opened at the

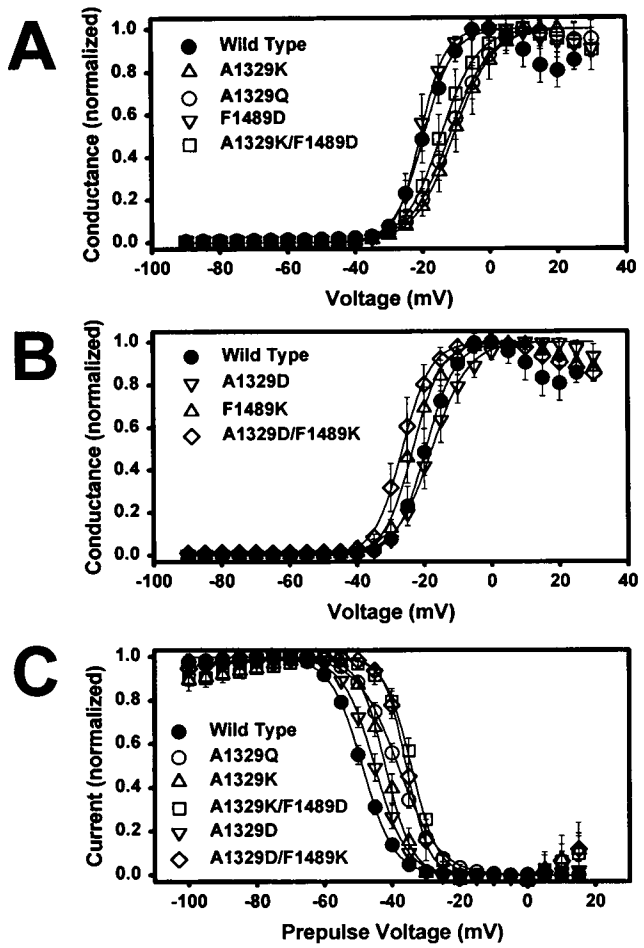

FIGURE 4 Voltage dependence of activation and inactivation. Conductance values for mutant and wild-type channels were determined and plotted as a function of depolarizing voltage, and the data were fit with a two-state Boltzmann equation, as described in Materials and Methods. Values for half-maximum activation ($V_{½}$) and effective gating charge (z) of the conductance curves are shown in Table 3. Symbols represent the means, and bars indicate standard deviations from n oocytes. The value for n is shown in Table 3 for each channel. (*A*) Voltage dependence of conductance for wild type (●), A1329K (△), A1329Q (○), F1489D (▽), and A1329K/F1489D (□). (*B*) Voltage dependence of conductance for wild type (●), A1329D (▽), F1489K (△), and A1329D/F1489K (◇). (*C*) The voltage dependence of inactivation was determined by using a 1-s prepulse, as described in Materials and Methods. Peak current amplitudes for mutant and wild-type channels were measured during the test depolarization, normalized to the maximum amplitude, and plotted as a function of the prepulse potential. The data were fit with a two-state Boltzmann equation as described in Materials and Methods. Values for half-maximum inactivation ($V_{½}$) and effective gating charge (z) of the inactivation curve are shown in Table 3 for mutant and wild-type channels. Symbols represent the means, and bars indicate the standard deviations from n oocytes. The value for n is shown in Table 3 for each channel.

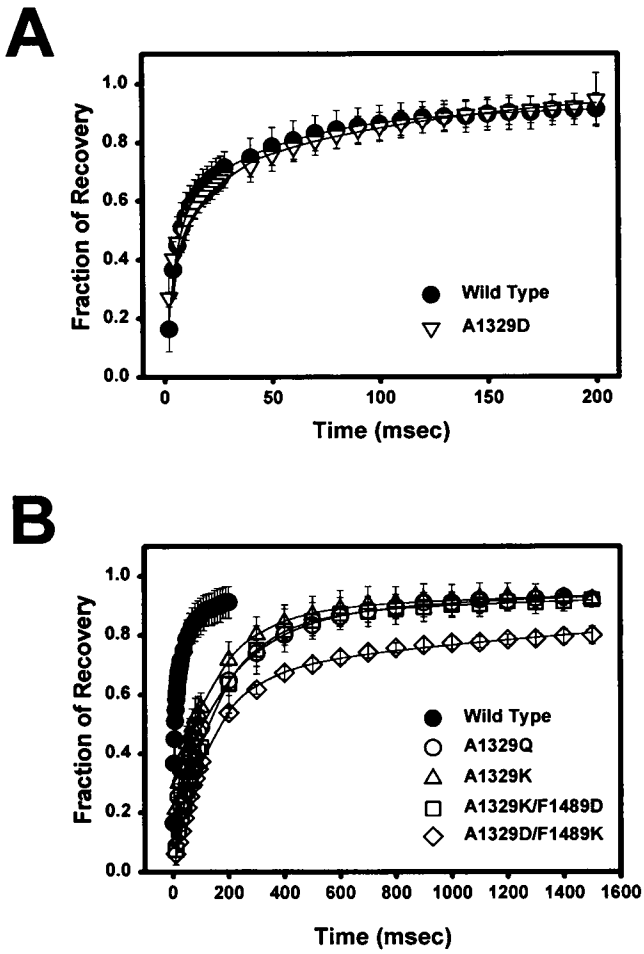

FIGURE 5 Recovery from inactivation. (*A*) Recovery from inactivation at a recovery potential of −100 mV for wild type (●) and A1329D (▽). The recovery period varied from 200 to 2 ms. The data were fit with either a double $(1 - [(a * \exp(-t/\tau 1) + b * \exp(-t/\tau 2)])$ or triple $(1 - [(a * \exp(-t/\tau 1) + b * \exp(-t/\tau 2) + c * \exp(-t/\tau 3)])$ exponential equation, as described in Materials and Methods. Symbols represent the means, and bars indicate the standard deviations from n oocytes. The value for n is shown for each channel in Table 3. (*B*) Recovery from inactivation with a variable recovery period from 1500 to 10 ms is shown for wild type (●), A1329Q (○), A1329K (△), A1329K/F1489D (□), and A1329D/F1489K (◇). The data were fit as described in *A*.

beginning of the depolarization, with a mean open time of 0.2 ms that is similar to that of the wild-type channel. A1329K/F1489D demonstrated several reopenings during the remainder of the depolarization that occurred more frequently than those of the A1329K mutant channel, and are reflected in the slight maintained current seen in the ensemble average. However, A1329K/F1489D has a transient peak open probability similar to that of the wild-type channel, with a maintained open probability that is significantly less than that of F1489D. These data indicate that the compensatory charges partially restored inactivation of the channel.

The rate constant for transitions out of the open state is equal to the inverse of the mean open time. The channel can leave the open state either by inactivating or by returning to the closed state. If we assume that the majority of channels inactivate rather than deactivate at −10 mV, as is the case during a strong depolarization in mammalian cells (Aldrich et al., 1983), then the transition rate constant reflects the transition from the open to the inactivated state. This transition for A1329K/F1489D is 50 times faster than that for

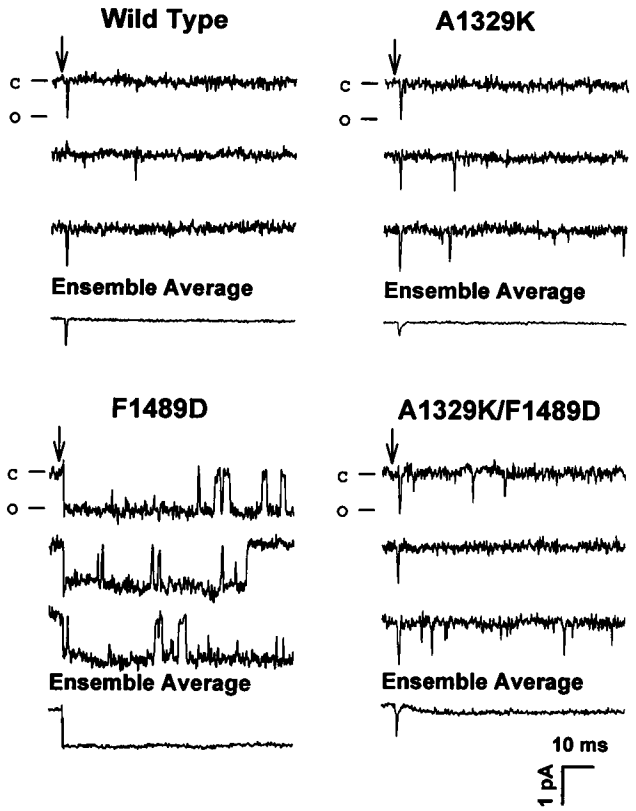

FIGURE 6 Representative single-channel currents for the wild-type, A1329K, F1489D, and A1329K/F1489D channels. Single-channel currents were recorded from inside-out patches of oocytes expressing the various mutant and wild-type sodium channels, as described in Materials and Methods. An arrow indicates the start of the depolarization to −10 mV from a holding potential of −100 mV. The closed and open states are indicated by a C and O, respectively. Ensemble averages are shown below the current traces for each channel. The number of traces used to calculate the ensemble average were as follows: wild type, 164; A1329K, 95; F1489D, 200; A1329K/F1489D, 337.

the F1489D mutant channel, and is not significantly different from that of the wild-type channel (Table 2). These data suggest that electrostatic interactions might be able to simulate hydrophobic interactions that could normally be occurring between A1329 and F1489 during inactivation.

Specificity of the interaction between F1489D and III S4-S5

Although glutamine substitutions at positions other than A1329 in domain III S4-S5 did not significantly affect the kinetics of inactivation, it was possible that the restoration of inactivation resulting from the compensatory charges might not be as specific. To examine the specificity of the interaction between the amino acids at positions 1489 and 1329, lysines were individually substituted for the hydrophobic residues two amino acids upstream (1327) or downstream (1331) from A1329. These mutations were then combined with F1489D to make the mutant channels V1327K/F1489D and L1331K/F1489D. Fig. 7 shows that

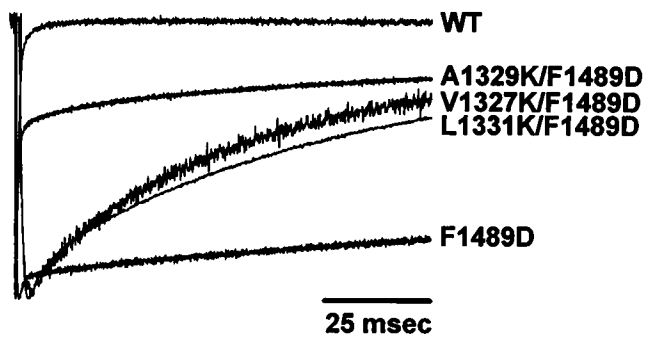

FIGURE 7 Specificity of the interaction between F1489D and III S4-S5. Representative current traces at a depolarization to −10 mV are shown for wild type (WT), F1489D, L1331K/F1489D, V1327K/F1489D, and A1329K/F1489D.

both V1327K/F1489D and L1331K/F1489D inactivated significantly faster than F1489D alone. However, both of these combination mutants inactivated more slowly than the A1329K/F1489D channel. The calculated "on" rate for the putative inactivation particle in A1329K/F1489D was faster than that for either V1327K/F1489D or L1331K/F1489D (Table 2). Interestingly, the "off" rate was also faster for A1329K/F1489D than for either V1327K/F1489D or L1331K/F1489D. This may result from a decrease in steric hindrance from the residues at positions 1327 and 1331, because in the wild-type channel larger residues occupy these positions (valine and leucine) compared to the alanine at position 1329. A decrease in steric hindrance may allow for increased stabilization of the lysine/aspartate interaction between F1489D and 1327K or 1331K, resulting in a slower "off" rate. These results demonstrate that positive charge replacements at multiple residues in III S4-S5 could partially restore inactivation to F1489D, but that a positive charge at position 1329 was more effective.

DISCUSSION

This study examines the importance of the S4-S5 linkers in domains II and III for inactivation of the rat brain type IIA sodium channel. Our results show that a highly conserved alanine at position 1329 in the S4-S5 linker of domain III is important for normal inactivation. Replacement of this alanine with a glutamine or a charged residue resulted in a channel with slower inactivation kinetics compared with those of the wild-type channel. The lack of any significant effects with the other mutations in domain II or III cannot be assumed to imply that no other residues in these regions are important for fast inactivation. We can only conclude that the substitution of glutamine residues at other positions in domains II and III did not significantly impair fast inactivation.

Previous studies have demonstrated that L_{III-IV} is essential for fast sodium channel inactivation, suggesting that the hydrophobic IFM residues in the linker form the nucleus of an inactivating particle (Patton et al., 1992; West et al., 1992; Kellenberger et al., 1997b). However, it has been

difficult to show that this putative inactivation particle interacts with another region of the channel to cause inactivation. Eaholtz et al. (1994) demonstrated that a peptide (KIFMK) can block sodium channels, but the sequence of this peptide is not contained within L_{III-IV}, because the flanking lysine residues are not present in the channel. Moreover, the properties of KIFMK block differ from those of fast inactivation (Tang et al., 1996). McPhee et al. (1994) have shown that mutations in domain IV S6 dramatically affect fast inactivation, but they concluded that this region does not function as a docking site because the KIFMK peptide could still inactivate the mutant channels (McPhee et al., 1995). In this report we have demonstrated that mutations in III S4-S5 can partially compensate for the inactivation defects of a mutation in L_{III-IV}, suggesting that these two regions of the channel interact with each other. The compensatory charge mutants A1329K/F1489D, A1329D/F1489K, A1329R/F1489E, and A1329E/F1489R inactivated significantly faster and more completely than F1489D, F1489K, F1489E, and F1489R. Furthermore, A1329K/F1489D had a single-channel mean open time that was similar to that of the wild-type channel and was ~50 times shorter than the mean open time for the mutant channel F1489D. These results suggest that a direct interaction between A1329 and F1489 is essential for complete sodium channel fast inactivation.

The interaction between L_{III-IV} and III S4-S5 is not dependent on the specific amino acid combination, but rather on the combination of opposite charged residues, as demonstrated by restoration of inactivation with both lysine/aspartate and arginine/glutamate combinations. However, the orientation of the charges did appear to have a significant effect on the extent of restoration of inactivation. By combining a positive charge in III S4-S5 with a negative charge in L_{III-IV}, we were able to restore inactivation more completely than when the charges were reversed. A1329R/F1489E inactivated most completely of all the compensatory charge mutant channels. A possible explanation for the more complete inactivation of this channel is that the A1329R mutation alone has a very minor effect on inactivation. Therefore, when A1329R is combined with F1489E, there may be less steric disturbance that would otherwise destabilize the charge interaction. The result that A1329R/F1489E had a much smaller K_{off} value than the other compensatory charge mutant channels is consistent with this hypothesis.

The interaction between F1489D and III S4-S5 does not require that the positive charge be specifically positioned at 1329. A positive charge at position 1327 or 1331 could also partially restore inactivation when combined with F1489D, as shown by the effects of the V1327K/F1489D and L1331K/F1489D double mutants. However, these double-mutant channels did not inactivate as rapidly as A1329K/F1489D. In addition, substitution of glutamine for either V1327 or L1331 had no effect on fast inactivation, suggesting that the hydrophobic interaction between F1489 and A1329 may be more specific in the wild-type channel than the electrostatic interaction between the charges in the double-mutant channels. The difference in specificity is consistent with the fact that hydrophobic interactions result from close-range interactions, whereas electrostatic interactions can have effects over a longer distance.

Many of the mutant channels differed in their voltage dependence of activation and steady-state inactivation when compared to the wild-type channel. Because activation and inactivation are coupled in the voltage-gated sodium channel, mutations that affect inactivation are likely to have effects on activation. The small changes in activation for channels with mutations in the III S4-S5 linker are not surprising, because the S4-S5 linkers are in close proximity to the S4 transmembrane segments that are involved in channel gating (Stühmer et al., 1989; Chen et al., 1996). However, the small shifts in the voltage dependence of conductance that were observed for the mutant channels cannot account for the large differences in inactivation kinetics between the channels with the compensatory charge mutations and the channels with a charge in only L_{III-IV}.

Many of the mutant channels recovered from fast inactivation more slowly than the wild-type channel. The slower recovery of the mutant channels can be explained by two possible mechanisms. First, in the context of the ball-and-chain model, the slower kinetics could suggest that these mutant channels have an inactivation particle that is binding more stably to its docking site compared to that of the wild-type channel. This could slow the transition from the inactivated to the closed state, reducing channel availability with successive depolarizations. This hypothesis is unlikely, because the K_{off} values for these channels were increased compared to those of the wild-type channels. Furthermore, the single-channel kinetics of A1329K and A1329K/F1489D showed that these channels have multiple openings during a depolarization, unlike the wild-type channel. Both of these results suggest that the putative inactivation particle is destabilized in its receptor site compared to the wild-type channel. A second hypothesis that may explain the slower recovery from inactivation is that the channels enter one of possibly many closed states after leaving the inactivated state at a hyperpolarized potential. It has previously been shown that the sodium channel must deactivate to a closed state to recover from fast inactivation (Kuo and Bean, 1994). The mutant channels may enter a more stable closed state, which would then delay entry back into the open state compared to the wild-type channel. This slower transition between closed states would result in a longer time before the channel could open, resulting in a longer recovery from inactivation.

The A1329K/F1489D channels demonstrated an ensemble average that is similar to that of the wild-type channel in the sense that there is an initial brief peak of current, but differs in the sense that there is also a maintained current (Fig. 6). In addition, the current appeared to decrease to the baseline after the initial peak, and then it increased again to a relatively stable maintained level. These characteristics were not observed in the macroscopic records (Fig. 3),

possibly because of the more limited time resolution of the two-electrode voltage clamp. We have carried out a preliminary comparison of the characteristics of the early openings that comprise the initial peak (within the first 10 ms) and the late openings that comprise the maintained current (after 10 ms). Neither the mean open times nor the amplitudes were significantly different in the two populations. One interpretation of these results is that the majority of channels open quickly and close relatively synchronously after the depolarization begins, after which they cannot reopen for a period of time. The synchronous opening and rapid closing would result in a peak of current that returns to baseline. Eventually, the channels would begin to reopen at a relatively constant rate, resulting in the maintained current. Consistent with this interpretation, ~70% of the channels opened within 2 ms after the depolarization started, and the mean closed time was 11.8 ms.

The transition rate from the open state to the inactivated state for A1329K/F1489D was shown to be ~50 times faster than that of F1489D and similar to the transition rate for the wild-type channel. However, single-channel recordings showed that A1329K/F1489D reopened several times during the duration of the depolarization, unlike the wild-type channel. The reopenings seen for A1329K/F1489D may be due to decreased stability of the inactivated state compared to its stability in the wild-type channel. These results are consistent with the faster "off" rate for A1329K/F1489D that was determined from whole-cell recordings. In the context of a ball-and-chain model, it is likely that a receptor site for the inactivation particle is multifaceted in sodium channels because there are four divergent domains. The A1329K mutant may eliminate one of several hydrophobic receptor sites for the inactivation particle, whereas a charge placed at F1489 likely disrupts interactions with all of the receptor sites. The A1329K/F1489D mutant may create one new charged receptor site that is able to interact electrostatically with the charged inactivation particle. Therefore, the transition rate from the open to the inactivated state for A1329K/F1489D is similar to that of the wild-type channel, but the transition rate from the inactivated state back to the open state is increased because of the instability caused by the remaining hydrophobic receptor sites.

Thermodynamic cycle analysis can be used to determine if two mutations are acting independently or interdependently (Carter et al., 1984; McPhee et al., 1995). The free energy of inactivation (ΔG) is a state function that depends only on the initial and final energies of the system and not on the path that is taken between the states. In this case, the four states of the system are wild type (WT), A1329K (K), F1489D (D), and A1329K/F1489D (KD) (Fig. 8). The sum of $\Delta(\Delta G)$ in either direction around the cycle must be the same, so that $\Delta(\Delta G)$ from WT→K + K→KD must equal the sum of $\Delta(\Delta G)$ from WT→D + D→KD. If A1329K and F1489D are acting independently, then the sum of $\Delta(\Delta G)$ from WT→K + WT→D should also equal the sum of $\Delta(\Delta G)$ from WT→K + K→KD. The values for ΔG were

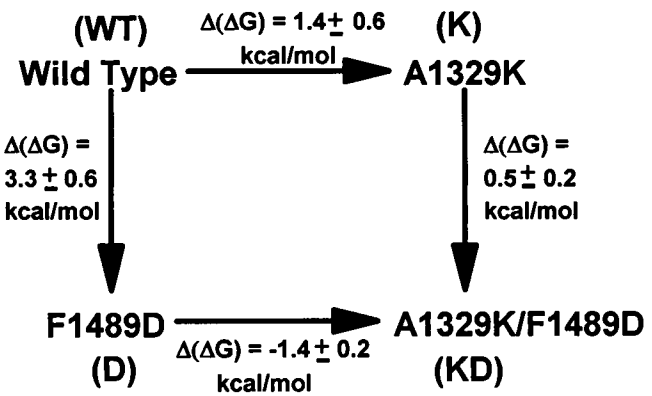

FIGURE 8 Thermodynamic analysis. Thermodynamic cycle analysis, showing the differences in ΔG of inactivation among the wild-type and mutant channels. For each channel, ΔG was calculated as described in Materials and Methods by using the K_{on} and K_{off} values in Table 2. The sum of $\Delta(\Delta G)$ from WT→K + K→KD equals the sum of the $\Delta(\Delta G)$ from WT→D + D→KD, as required for a thermodynamic cycle. The sum of $\Delta(\Delta G)$ from WT→K + WT→D does not equal the sum of $\Delta(\Delta G)$ from WT→K + K→KD, indicating that the effects of the mutations on ΔG of inactivation are not independent.

calculated for wild-type and mutant channels, as described in Materials and Methods, using the K_{on} and K_{off} rates in Table 2. Similar results were obtained for analyses using rates calculated for depolarization to both −10 mV and +100 mV (data not shown). The sum of $\Delta(\Delta G)$ from WT→K + WT→D is equal to 4.7 ± 0.6 kcal/mol, whereas the sum of $\Delta(\Delta G)$ from WT→K + K→KD is equal to 1.9 ± 0.6 kcal/mol. The difference between the two values, which is 2.8 kcal/mol, is considered the coupling energy between the two mutations (Carter et al., 1984). Therefore, these two pathways result in significantly different changes in free energy from the initial to the final states. A coupling energy of similar magnitude (2.0 kcal/mol) was observed for the combination of A1329E and F1489R mutations (data not shown). These results indicate that the A1329K and F1489D mutations are not independent. Rather, the ΔG of inactivation for the F1489D channels varies, depending on the presence of the A1329K mutation, demonstrating an interaction between A1329K and F1489D to result in a channel that inactivates faster than for F1489D alone.

In conclusion, these data show that the alanine at position 1329 in the S4-S5 linker of domain III interacts with position 1489 in $L_{III\text{-}IV}$. Considered in the context of the ball-and-chain model, the results are consistent with the hypothesis that A1329 forms part of the docking site for the $L_{III\text{-}IV}$ fast inactivation particle. Future studies are necessary to identify other regions that may form the docking site for the fast inactivation particle, and to test the validity of the ball-and-chain model for sodium channel inactivation.

We thank Drs. Linda Hall, Kris Kontis, Michael Pugsley, Ray Smith, and Ted Shih for helpful discussions during the course of this work, and Bonnie Lerner and Mimi Reyes for excellent technical assistance.

Supported by National Institutes of Health research grant NS26729 and a grant from the National Multiple Sclerosis Society. ALG is an Established Investigator of the American Heart Association.

REFERENCES

Aldrich, R. W., D. P. Corey, and C. F. Stevens. 1983. A reinterpretation of mammalian sodium channel gating based on single channel recording. *Nature.* 306:436–441.

Armstrong, C. M., and F. Bezanilla. 1977. Inactivation of the sodium channel. II. Gating current experiments. *J. Gen. Physiol.* 70:567–590.

Auld, V. J., A. L. Goldin, D. S. Krafte, W. A. Catterall, H. A. Lester, N. Davidson, and R. J. Dunn. 1990. A neutral amino acid change in segment IIS4 dramatically alters the gating properties of the voltage-dependent sodium channel. *Proc. Natl. Acad. Sci. USA.* 87:323–327.

Carter, P. J., G. Winter, A. J. Wilkinson, and A. R. Fersht. 1984. The use of double mutants to detect structural changes in the active site of the tyrosyl-tRNA synthetase (*Bacillus stearothermophilus*). *Cell.* 38: 835–840.

Catterall, W. A. 1992. Cellular and molecular biology of voltage-gated sodium channels. *Physiol. Rev.* 72:S15–S48.

Chen, L.-Q., V. Santarelli, R. Horn, and R. Kallen. 1996. A unique role for the S4 segment of domain 4 in the inactivation of sodium channels. *J. Gen. Physiol.* 108:549–556.

Eaholtz, G., T. Scheuer, and W. A. Catterall. 1994. Restoration of inactivation and block of open sodium channels by an inactivation gate peptide. *Neuron.* 12:1041–1048.

Goldin, A. L. 1991. Expression of ion channels by injection of mRNA into *Xenopus* oocytes. *Methods Cell Biol.* 36:487–509.

Goldin, A. L. 1995. Voltage-gated sodium channels. *In* Ligand- and Voltage-Gated Ion Channels. R. A. North, editor. CRC Press, Boca Raton, FL. 73–112.

Hoshi, T., W. N. Zagotta, and R. W. Aldrich. 1990. Biophysical and molecular mechanisms of *Shaker* potassium channel inactivation. *Science.* 250:533–538.

Isacoff, E. Y., Y. N. Jan, and L. Y. Jan. 1991. Putative receptor for the cytoplasmic inactivation gate in the *Shaker* K^+ channel. *Nature.* 353: 86–90.

Isom, L. L., K. S. DeJongh, D. E. Patton, B. F. X. Reber, J. Offord, H. Charbonneau, K. Walsh, A. L. Goldin, and W. A. Catterall. 1992. Primary structure and functional expression of the β_1 subunit of the rat brain sodium channel. *Science.* 256:839–842.

Kellenberger, S., T. Scheuer, and W. A. Catterall. 1996. Movement of the Na^+ channel inactivation gate during inactivation. *J. Biol. Chem.* 271: 30971–30979.

Kellenberger, S., J. W. West, W. A. Catterall, and T. Scheuer. 1997a. Molecular analysis of potential hinge residues in the inactivation gate of brain type IIA Na^+ channels. *J. Gen. Physiol.* 109:607–617.

Kellenberger, S., J. W. West, T. Scheuer, and W. A. Catterall. 1997b. Molecular analysis of the putative inactivation particle in the inactivation gate of brain type IIA Na^+ channels. *J. Gen. Physiol.* 109:589–605.

Kontis, K. J., and A. L. Goldin. 1993. Site-directed mutagenesis of the putative pore region of the rat IIA sodium channel. *Mol. Pharmacol.* 43:635–644.

Kuo, C.-C., and B. P. Bean. 1994. Na^+ channels must deactivate to recover from inactivation. *Neuron.* 12:819–829.

McClatchey, A. I., P. Van den Bergh, M. A. Pericak-Vance, W. Raskind, C. Verellen, D. McKenna-Yasek, K. Rao, J. L. Haines, T. Bird, R. H. Brown, Jr., and J. F. Gusella. 1992. Temperature-sensitive mutations in the III-IV cytoplasmic loop region of the skeletal muscle sodium channel gene in paramyotonia congenita. *Cell.* 68:769–774.

McPhee, J. C., D. S. Ragsdale, T. Scheuer, and W. A. Catterall. 1994. A mutation in segment IVS6 disrupts fast inactivation of sodium channels. *Proc. Natl. Acad. Sci. USA.* 91:12346–12350.

McPhee, J. C., D. S. Ragsdale, T. Scheuer, and W. A. Catterall. 1995. A critical role for transmembrane segment IVS6 of the sodium channel α subunit in fast inactivation. *J. Biol. Chem.* 270:12025–12034.

Moorman, J. R., G. E. Kirsch, A. M. Brown, and R. H. Joho. 1990. Changes in sodium channel gating produced by point mutations in a cytoplasmic linker. *Science.* 250:688–691.

Murrell-Lagnado, R. D., and R. W. Aldrich. 1993a. Interactions of amino terminal domains of Shaker K channels with a pore blocking site studied with synthetic peptides. *J. Gen. Physiol.* 102:949–975.

Murrell-Lagnado, R. D., and R. W. Aldrich. 1993b. Energetics of Shaker K channels block by inactivation peptides. *J. Gen. Physiol.* 102: 977–1003.

Patton, D. E., and A. L. Goldin. 1991. A voltage-dependent gating transition induces use-dependent block by tetrodotoxin of rat IIA sodium channels expressed in *Xenopus* oocytes. *Neuron.* 7:637–647.

Patton, D. E., J. W. West, W. A. Catterall, and A. L. Goldin. 1992. Amino acid residues required for fast sodium channel inactivation. Charge neutralizations and deletions in the III-IV linker. *Proc. Natl. Acad. Sci. USA.* 89:10905–10909.

Patton, D. E., J. W. West, W. A. Catterall, and A. L. Goldin. 1993. A peptide segment critical for sodium channel inactivation functions as an inactivation gate in a potassium channel. *Neuron.* 11:967–974.

Ptacek, L. J., R. Tawil, R. C. Griggs, G. Meola, P. McManis, R. J. Barohn, J. R. Mendell, C. Harris, R. Spitzer, F. Santiago, and M. F. Leppert. 1994. Sodium channel mutations in acetazolamide-responsive myotonia congenita, paramyotonia congenita, and hyperkalemic periodic paralysis. *Neurology.* 44:1500–1503.

Smith, R. D., and A. L. Goldin. 1996. Phosphorylation of brain sodium channels in the I-II linker modulates channel function in *Xenopus* oocytes. *J. Neurosci.* 16:1965–1974.

Stühmer, W., F. Conti, H. Suzuki, X. Wang, M. Noda, N. Yahagi, H. Kubo, and S. Numa. 1989. Structural parts involved in activation and inactivation of the sodium channel. *Nature.* 339:597–603.

Tang, L., R. G. Kallen, and R. Horn. 1996. Role of an S4–S5 linker in sodium channel inactivation probed by mutagenesis and a peptide blocker. *J. Gen. Physiol.* 108:89–104.

Vassilev, P., T. Scheuer, and W. A. Catterall. 1989. Inhibition of inactivation of single sodium channels by a site-directed antibody. *Proc. Natl. Acad. Sci. USA.* 86:8147–8151.

Wang, D. W., K. Yazawa, A. L. George, Jr., and P. B. Bennett. 1996. Characterization of human cardiac Na^+ channel mutations in the congenital long QT syndrome. *Proc. Natl. Acad. Sci. USA.* 93: 13200–13205.

Wang, Q., J. Shen, I. Splawski, D. Atkinson, Z. Li, J. L. Robinson, A. J. Moss, J. A. Towbin, and M. T. Keating. 1995. *SCN5A* mutations associated with an inherited cardiac arrhythmia, long QT syndrome. *Cell.* 80:805–811.

West, J. W., D. E. Patton, T. Scheuer, Y. Wang, A. L. Goldin, and W. A. Catterall. 1992. A cluster of hydrophobic amino acid residues required for fast Na^+ channel inactivation. *Proc. Natl. Acad. Sci. USA.* 89: 10910–10914.

Yang, N., S. Ji, M. Zhou, L. J. Ptacek, R. L. Barchi, R. Horn, and A. L. George, Jr. 1994. Sodium channel mutations in paramyotonia congenita exhibit similar biophysical phenotypes in vitro. *Proc. Natl. Acad. Sci. USA.* 91:12785–12789.

Zagotta, W. N., T. Hoshi, and R. W. Aldrich. 1990. Restoration of inactivation in mutants of *Shaker* potassium channels by a peptide derived from ShB. *Science.* 250:568–571.